Post-print version of the paper published in Energy and Buildings, Volumes 188–189, 1 April 2019, Pages 1-11, doi: https://doi.org/10.1016/j.enbuild.2019.02.004

Nano-encapsulation of phase change materials: from design to thermal performance, simulations and toxicological assessment

Valeria De Matteis[1] Alessandro Cannavale[2,3], Francesco Martellotta[2], Rosaria Rinaldi[1], Paola Calcagnile[4], Francesca Ferrari[4], Ubaldo Ayr[2], Francesco Fiorito[5*]

1. Dipartimento di Matematica e Fisica “Ennio De Giorgi”, Università del Salento, Via Monteroni, Lecce, Italy

2. Dipartimento di Scienze dell'Ingegneria Civile e dell'Architettura (DICAR), Politecnico di Bari, via Orabona, Bari, Italy

3. CNR Nanotec, Istituto di Nanotecnologia, via Arnesano, Lecce, Italy

4. Dipartimento di Ingegneria dell’Innovazione, Università del Salento, via Monteroni, Lecce, Italy

5. Dipartimento di Ingegneria Civile, Ambientale, del Territorio, Edile e di Chimica (DICATECh), Politecnico di Bari, via Orabona, Bari, Italy

*corresponding author

Abstract

The paper presents the results of an experimental activity aimed at producing and characterizing a nano-encapsulated PEG600 (PCMs) into a silica shell. The nano-encapsulation was meant to be useful to improve the material’s suitability to integration in building components. The (300 ± 15) nm nanoparticles that were produced underwent a full characterization of their thermal performances. An enthalpy of fusion as high as 66.24 kJ/kg, in a tight melting temperature range (20-21°C) was obtained, making the material suitable for thermal energy storage in buildings. In order to demonstrate the benefits of such as this technology on the reduction of heating and cooling demand of buildings, a concentration of 50% in weight of nanoparticles was, then, embedded into a gypsum plasterboard and used for all indoor plastered surfaces of a reference residential buildings. A saving of respectively up to 4.3% and up to 1.1% of heating and cooling energy demand was predicted in comparison to the ones of a building without PCM. Finally, the material underwent a full toxicological characterization exposing human alveolar basal epithelial cells to nanoparticles. The results showed that there were no toxic effects on cell morphology.

Nomenclature

PCM	Phase Change Material
NP	Nanoparticle
USD	United States Dollars
PEG	Polyethylene glycol
SiO_2	Silicon Dioxide

Post-print version of the paper published in Energy and Buildings, Volumes 188–189, 1 April 2019, Pages 1-11, doi: https://doi.org/10.1016/j.enbuild.2019.02.004

TEOS	Tetraethyl orthosilicate
NH_4OH	Ammonium hydroxide
SiO_2@PEG600	Nanoencapsulated PEG600 in SiO_2 shells
TEM	Transmission Electron Microscopy
EDS	Energy Dispersive X-ray Spectroscopy
DLS	Dynamic Light Scattering
SEM	Scanning Electron Microscopy
IR	Infrared
FT-IR	Fourier-Transform IR Spectroscopy
DSC	Differential Scanning Calorimetry
T_m	Melting Temperature of a PCM (°C)
ΔH_m	Total Enthalpy of fusion (kJ)
Δh_m	Enthalpy of fusion per unit mass (kJ/kg)
U_f	Frame global heat transfer coefficient (W/m^2K)
U_g	Glazing global heat transfer coefficient (W/m^2K)
S	Superscript indicating the solid phase
L	Superscript indicating the liquid phase

1. Introduction

In the last decade, the potential integration of PCMs in building components, as suitable latent thermal energy storage systems, has become a goal for several research activities. PCMs can store large amounts of latent heat in their phase transitions [1], achieving significant energy savings and comfort in buildings. If, on the one hand, sensible heat refers to heat that can be sensed by means of a thermometer, latent heat storage refers to the undetectable heat transfer, intrinsically associated with a phase transition [2]. PCMs can utilise their high latent heat storage, corresponding to the number of chemical bonds to be broken to activate the full isothermal phase transition at constant pressure. For this reason, within the tight temperature range in which the phase transition occurs, PCMs show higher efficiency than any other sensible heat storage material [3]. PCMs are classified in three classes: organic, inorganic and eutectic [3]: organic PCMs are paraffins, fatty acids, esters, and alcohols [4] while the most used inorganic PCMs are salt hydrates. Metallic PCMs, that are classified as inorganic, are rarely used in buildings due to their weight and high melting temperature. Generally, higher melting temperatures are reported for metals and inorganic PCMs, whereas they are lower in organic, salt hydrate and eutectic PCMs [5]. The main figures of merit affecting PCMs effectiveness are the melting temperature, the amount of latent heat of transition per unit weight, thermal conductivity (λ) and the specific heat. Shape-stabilized PCMs, by means of micro- and nano-encapsulation processes, avoid any leakage risk in the liquid phase, but also maximize heat transfer due to larger available surface area, compared to macrocapsules [6]. Micro-encapluation is a technology to encapsulate and shape-stabilize PCMs in spheres at microscale range (> 1μm); the current research trend is aimed at reducing the encapsulation size within the nanoscale range, so as to maximize size effects and surface area involved in heat transfer [7].

PCMs can help customizing the redistribution of thermal loads in buildings. A recent review showed that generally PCMs are embedded in building elements and materials, especially in walls and floor elements, because they can provide energy storage by means of latent heat accumulation, resulting in higher heating storage with respect to typical sensible heat processes of building materials [8]. The improvement observed in PCM-embodying elements is due to this enhanced latent heating storage, even if no variation of specific heats takes place. For instance, the application of PCM capsules with paraffinic wax in lime plaster enhanced the apparent specific heat capacity, compared to the reference material [9]. PCM-enhanced plasters have been investigated as a suitable chance in the refurbishment of building envelopes, in the Mediterranean climate [10], in the hypothesis of adopting 3.0 cm thick plaster on all exposures and in different climatic conditions. The heat storage capacity of a special composite plaster was compared to a commercially produced lime-cement mortar, reporting an increase from 0.4 kJ/(kg·K) to about 2.1 kJ/(kg·K) after the addition of 24% PCM [11]. Pavlick et al. [12], in 2014, reported the enhanced performance of a PCM-modified plaster exhibiting specific heat capacity of 1.6 kJ/(kg·K) against 0.77 kJ/(kg·K) observed in the reference plaster. The integration of PCMs in lightweight building components was investigated by Fiorito [13], employing EnergyPlus for simulating the use of PCMs in a naturally ventilated test room. In that study, higher benefits were obtained by adding PCMs in walls or partitions, linearly with PCM thickness. Lee and Medina [14] simulated a frame wall embodying hydrated salt (melting and solidification temperatures between 27.6 °C–29.6 °C) macroencapsulated in containers larger than 1 mm. The aim was to reduce the cooling on-peak demand in California. Total energy saving reached values of 9.21 kWh/(m^2·yr) due to PCM-enhanced frame walls. Energy saving between 30% and 55% in the HVAC system were registered by Navarro et al. [15], who used an internal slab as a storage unit and as an active cooling supply in Spain. They used 52 kg of RT-21 paraffin macro-encapsulated in 1456 aluminium tubes of 12 mm diameter. Kenisarin et al. observed that further research activities on PCMs should, among the other objectives, achieve the narrowest possible temperature range for the phase change process in PCMs and reduce their costs [16]. Several research groups used paraffin, as reviewed by Zalba et al. [17] for its melting temperature (for instance, paraffin wax has a melting temperature of 28 °C) and its high latent heat (244 kJ/kg), highly compatible with uses in constructions.

Nanotechnologies can help enhancing PCMs performance, as a natural evolution, since abrupt changes may occur, at nanoscale level, in thermophysical and physicochemical properties. Then nano-enhanced features of PCM materials could be suitably exploited and several research activities are currently working on this point, as reviewed by Parameshwaran [18]. It has been observed that the inclusion of nanomaterials could improve some PCMs figures of merit, overcoming some of their limitations, such as a low value of thermal conductivity [19]. To this aim, several nano-enhanced PCMs have been proposed, embodying, for instance, copper, titania, alumina, silica and zinc oxide nanoparticles (NPs), thoroughly investigated by Teng et al. [20]: they showed that titania NPs are more effective than other additives in order to enhance heat conduction and thermal storage capacity in paraffins, also affecting both melting onset temperature and the solidification temperature. A completely different route to nano-enhancement of PCMs consists in their encapsulation within a nano-shell [21] or a nanofiber [22]. In addition, nano-shells protect PCMs from the surrounding environment. Liu et al. [23] described the different routes to synthetize different kinds of nano-PCMs (sol-gel, miniemulsion, emulsion and *in situ* polymerization) and the respective advantages and disadvantages. Sari et al. [24] synthetized polystyrene and n-heptadecane micro-/nanocapsules adopting the emulsion polymerization route with capsule sizes ranging from 10 nm to 40 mm for a 1:2 ratio of polystyrene and n-heptadecane. However, among different materials to be used for encapsulation, amorphous silica shows high heat storage capacity and thermal conductivity [25]. In addition, it is biocompatible, nontoxic for living organisms and the environment [26,27], and in its core it is easy to confine active molecules acting as reservoir [28]. Zhang et al. [29] synthesized silica spheres (7–16 µm) with *n*-octadecane core (melting temperature range of 23–28 °C) using TEOS as an inorganic precursor by a sol–gel process, with different steps. The obtained nanomaterials showed a good thermal conductibility. Similarly, Belessiotis et al. [30] obtained silica spheres with paraffin core via sol gel method showing a latent heat of ~ 156 kJ/kg. Latibari et al. [31] obtained nano-PCMs with palmitic acid core and silica shell, using multistep sol-gel method and investigated their thermal figures. The efficiency of encapsulation, defined as the percent ratio of the latent heat of the encapsulated PCM and that of the pure PCM, ranged from 83.25% to 89.55% (with a particle size between 183.7 nm and 722 nm) depending on pH of the chemical mix solution. Nevertheless, since palmitic acid has a melting temperature of 61°C, the application in buildings is quite difficult. The same limitation (high melting temperature ranging from 142.1 °C to 166.2 °C) concerned mannitol, chosen by Wu et al. [32] and Pethurajan et al. [33].

The cost-effectiveness of PCMs inclusion in building envelopes was investigated by Kosny et al. [34], who found that the commercial cost of a PCM with a latent heat as high as 116 kJ/kg, while produced commercially, can be projected to be 4.4-6.6 USD/kg. On the other hand, PCMs for building applications should be produced by means of environmental-friendly processes and raw materials. Among the possible PCMs, paraffin is inflammable and it is classified as a doubtful carcinogen (source: Sigma-Aldrich), while PEG is an inert inexpensive and versatile polymer for customizing nanostructured materials due to its intrinsic biocompatibility and water solubility [35]. It is also widely used in the biomedical field and it has been approved by Food and Drug Administration for many applications [36]. In addition, the range of melting temperature is between 17 and 22°C (Source: Sigma-Aldrich), that is well within the range of comfortable indoor environment temperatures and, for this reason, its application in buildings is preferable.

In this work, we obtained (300 ± 15) nm SiO_2@PEG600NPs by means of a one step, easy and reproducible synthetic route. The obtained nanostructures were then fully characterized, before undergoing a toxicological assessment. The SiO_2@PEG600NPs showed a good thermal performance, with an enthalpy of fusion as high as 66.24 kJ/kg, in the tight melting temperature range (20-21°C): such feature makes it a good candidate for thermal energy storage in building applications, especially to reduce energy uses during winter season HVAC. As will be seen hereafter, it is precisely during the winter season that the incorporation of the PCM inside the plaster performs its effectiveness. On the contrary, during the summer season, it shows no particular benefit, mainly because the temperature of the internal surface of the vertical walls is almost always above the T_m of the PCM. Following the experimental design and synthesis activities of the nanostructures incorporating PCMs, we performed dynamic simulations able to show the possible extent of energy savings obtained by integrating a certain percentage of SiO_2@PEG600NPs (50%) in building gypsum plasters, comparing a reference case, devoid of PCM, with another one, containing the proposed material applied over all internal vertical plastered surfaces. It is the case to specify that the choice of PEG600 as a suitable PCM was carried out following a tight comparison aimed at identifying a material having, at the same time, different specificities. Firstly, the compatibility with a low-cost synthesis mode of the hosting SiO_2 shell; secondly, it represented a biocompatible PCM and, finally, a series of preventive simulation activities (not reported in the text) provided an ideal range of melting temperatures to make the maximum contribution during the winter season, associated to the maximum benefit in terms of energy saving. After all these considerations and activities, we decided to adopt the PEG600 as a material able to guarantee a satisfactory compromise.

2. Materials and Methods

In this experimental activity we have reported the results of a cross-disciplinary design and the full characterization of a novel nanostructured material, showing the advantage of achieving full shape stabilization of a biocompatible PCM (PEG600) within the nanoscale, inside a non-toxic amorphous SiO_2 shell. The main properties of this specially designed material were fully characterized after the chemical synthesis. To this aim, at first microscopy characterization was carried out to observe shape and size of nanoparticles; then, thermal characterization was experienced in order to know the main figures of merit describing PCMs behaviour. The last step was an in vitro toxicological assessment: this last characterization activity was carried out in order to learn if the material presented significant toxicity and, therefore, risk profiles for human health. Data thus obtained were used as an input for the subsequent simulation activities.

2.1 Synthesis and characterization of SiO_2@PEG600

The synthesis was carried out adopting the so called Stöber method, following the procedure described in Stöber et al. [37] with some modifications in order to encapsulate PCM_S materials. An amount of PEG600 was dissolved in 5 mL of ethanol to obtain a solution of PEG600 concentrated at 1 mM in final volume of reaction. To ethanol-PEG600 solution was added TEOS (100 µL), milliQ water (20 mL) and NH_4OH solution (28.0-30.0%, 10 mL) for 2 hours at 25°C (this temperature was optimal to maintain PEG600 in the liquid phase). Then, the reaction was blocked with acetone and the solution is centrifuged at 4000 rpm for 20 minutes. The SiO_2@PEG600 NPs were rinsed with milliQ water and ethanol (1:1) 5 times and successively dried under reduced pressure and then at 100 °C for 2 h in order to obtain a white nano-powder. The yield for this synthesis was about 80%.

TEM characterization was carried out by means of a JEOL Jem 1011 microscope, operating at an accelerating voltage of 100 kV (JEOL USA, Inc). TEM samples were prepared by dropping a dilute solution of NPs in water on carbon-coated copper grids (Formvar/Carbon 300 Mesh Cu).

DLS and ζ-potential measurements were performed on a Zetasizer Nano-ZS equipped with a 4.0 mW HeNe laser operating at 633 nm and an avalanche photodiode detector (Model ZEN3600, Malvern Instruments Ltd., Malvern, UK).

SEM and EDS Measurements were recorded using a Phenom ProX microscope (Phenom-World B. V., Eindhoven, Germany), at an accelerating voltage of 10 kV. The samples were prepared by dropping a solution of NPs in water on monocrystalline silicon wafer.

FT-IR analysis on SiO_2@PEG600 were recorded on a JASCO 660 plus infrared spectrometer (Jasco, Gross-Umstadt, Germany). Spectral manipulations were performed using the spectral analysis software provided by Jasco and spectra were acquired in the number wave range of 4000-650 cm^{-1} (resolution of 4 cm^{-1}) at room temperature on a square micro aperture of 100 µm, with the accumulation of 100 repeated scans in reflectance mode. An isopropanol-treated silicon wafer was used, as background.

Thermal properties of SiO_2@PEG600, such as T_m, T_f and ΔH_m, were measured by means of a DSC instrument (Mettler Toledo 822, Greifensee, Switzerland). The analysis was performed on dried samples under a constant stream of nitrogen (60 mL • min^{-1}) at atmospheric pressure, applying a first isothermal step at -10 °C for 5 minutes, followed by a heating scan between -10 °C and 90 °C at 1 °C • min^{-1}. Then the samples were submitted to a further isothermal step at 90°C for 5 minutes, followed by a cooling scan from 90 °C to -10°C at 1°C • min^{-1}. The phase change temperatures (melting and freezing points) were evaluated as the intersection between the tangent to the maximum rising slope of the peak and the sample baseline. The enthalpies related to the phase changes were determined by integration of the area under the peaks *versus* time.

2.2 Dynamic simulations in a case study

In order to test the potential benefits resulting from the use of the proposed PCM, a typical Italian dwelling, located in a multi-storey building, was modelled in EnergyPlus (Figure 1). The overall floor surface is 78 m^2 and the internal height is 2.9 m. Its East and West walls are shared with other apartments. The dividing walls are made of 20 cm thick tufa blocks, with plaster on both faces (U=0.622 W/m^2K). Internal walls are made of 10 cm thick tufa blocks with plaster on both sides. Floor and ceiling are 30 cm thick and are made of hollow clay blocks covered with concrete and plaster on the bottom face (U_{floor}=0.819 W/m^2K,

Post-print version of the paper published in Energy and Buildings, Volumes 188–189, 1 April 2019, Pages 1-11, doi: https://doi.org/10.1016/j.enbuild.2019.02.004

U_{ceil}=0.857 W/m^{2}K). Heat exchange takes place through the North and South walls, made of hollow clay blocks (30 cm thick), and through the west wall facing the stairway, which is also made of clay blocks (U=0.736 W/m^{2}K). Windows embody a 70 mm PVC frame (U_f=1.2 W/m^{2}K) and a glazing system made of two 4 mm panes, divided by a 20 mm air gap (U_g=2.7 W/m^{2}K). The values of global coefficient of heat exchange have been kept constant both in the reference case and in the model embodying PCMs within the internal plasters of vertical walls. This was done precisely in order to highlight the contribution of the PCMs on energy consumption for HVAC. Moreover, ceiling and internal floor did not include PCMs and the only non-adiabatic surfaces, therefore involved in the heat transmission mechanisms, were the vertical walls respectively exposed to North and South, as shown in Figure 1.

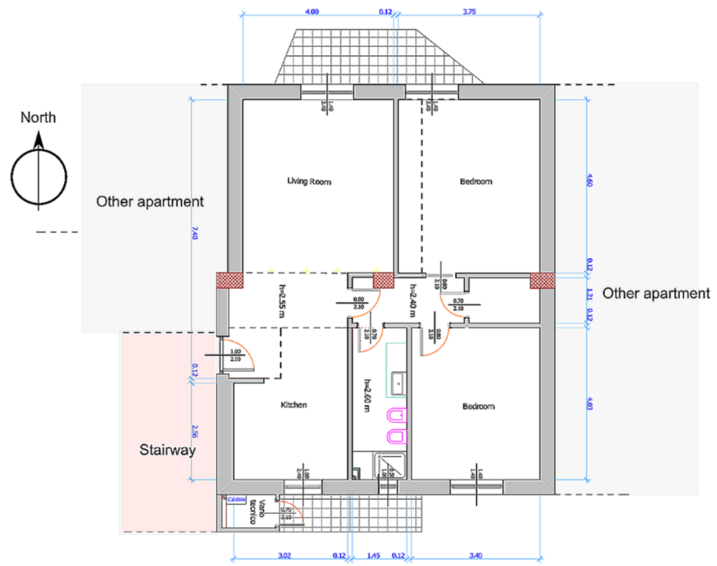

Figure 1. Plan of the apartment used to create the EnergyPlus model

2.2.1 The EnergyPlus model

A 3D model of the case study was first made in SketchUp using the OpenStudio plugin, and subsequently exported to EnergyPlus v. 8.8, a free simulation tool by the U.S. Department of Energy's Building Technology Office, in order to perform the dynamic energy analysis. To assess the heating and cooling energy uses in a simplified way, an "IdealLoadAirSystem" with no outdoor air was considered. Adopting this approach, EnergyPlus provides heating and cooling energy required to meet the temperature at the selected setpoints (20.5 °C in winter, 26 °C in summer). This approach allows to calculate the thermal energy strictly necessary to achieve the comfort objectives represented by the temperature setpoints. In this way, we obtain the advantage of highlighting the free contribution of the material, neglecting the optimization effects of real HVAC systems.

However, in order to better simulate the actual transients that typically occur in real houses, the duty cycle of the heating thermostat was simulated by means of an Energy Management System so that the heating was turned off when air temperature was above $T_{setpoint}$+0.5 °C, while it was turned on when air temperature fell below $T_{setpoint}$–0.5 °C.

For ventilation, in order to simulate the actual opening cycles of windows in real conditions of use, the "Wind and Stack Open Area" approach was adopted in EnergyPlus, which allows to provide the effective opening surface on the respective exposures. Windows (having an open area of 0.4 m^2 for both Northern and Southern façades) were supposed to be open half an hour per day (from 7.30 to 8.00) during workdays, and one hour per day during weekends. In addition, for fixed openings and windows cracks (summing up to 0.03 m^2 area) an “always on” schedule was applied.

Simulations were carried out in three Italian cities belonging to different climatic zones: Brindisi (climatic zone C, 1083 heating degree days), Rome (climatic zone D, 1415 heating degree days), and Milan (climatic zone E, 2404 heating degree days). The heating schedule was adapted to each location, according to the climatic zone they belonged to, depending on national regulations (Figure 2). The definition of such climatic zones is carried out according to the concept of heating degree day, i.e. the sum of the daily thermal excursions extended to the winter heating period. The latter period is established by regulations in force. According to the Italian standard, all municipalities with a number of degree days between 900 and 1400 are in zone C; the range of values for the D climatic zone is between 1400 and 2100 and between 2100 and 3000 for the E climatic zone.

Thus, in Brindisi heating worked from November 15th to March 31st, with up to 8 hours per day. In Rome heating worked from November 1st to April 15th with a maximum of 10 hours per day, and in Milan from October 15th to April 15th with a maximum of 12 hour per day. Cooling was considered to be turned on from July 1st to August 31st in all the locations. Envelope thermal resistance was considered unvaried, although climate zones were significantly different.

Among the different output variables that can be returned by the software, 60 seconds timestep simulations (using conduction finite difference method ConFD, required for simulations involving PCMs) and hourly values of surface temperature were considered as more useful and instructive for the case under investigation. Overall values were employed for heating energy.

Post-print version of the paper published in Energy and Buildings, Volumes 188–189, 1 April 2019, Pages 1-11, doi: https://doi.org/10.1016/j.enbuild.2019.02.004

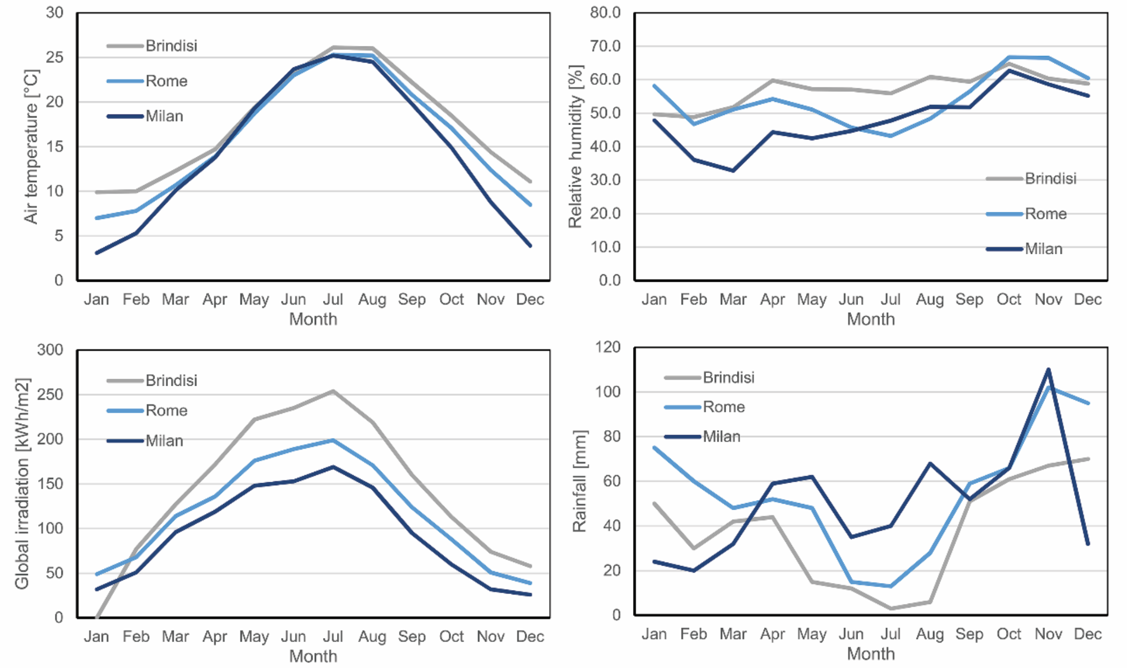

Figure 2. Monthly averages of climatic parameters for the three selected cities: a) Dry bulb outdoor temperature; b) Relative humidity; c) Global irradiation on horizontal surface; d) Rainfall. (Data source: Meteonorm 7.2)

The two horizontal surfaces as well as the Eastern and Western walls were considered adiabatic, so that all the other surfaces were modelled to simulate a room laying in an intermediate floor. However, although not involved in heat exchange, their density, heat capacity and conductivity were provided, in order to take into account their contribution to internal mass and heat storage.

In order to evaluate the thermal and energy benefits attainable including nano-PCMs in building components and materials, a typical masonry in hollow clay blocks covered with plaster on both sides was used for modelling external walls. PCMs were included in the internal plaster layer (with a thickness of 5 cm) of vertical surfaces, also in partitions. The total enthalpy of fusion of nano-encapsulated PCMs embodied in plasters, used for the simulations, was calculated adding the sensitive and latent contributions of the specific enthalpy. The total enthalpy of nano-enahnced plaster was then calculated as follows:

$$\Delta H_{tot} = m\,(\Delta h_{mortar} + \Delta h_{PCM}) \quad [\text{kJ}] \qquad (1)$$

where:

$$\Delta h_{mortar} = (1-f)\int_{T_1}^{T_2} c\,dT \qquad (2)$$

$$\Delta h_{PCM} = f\left[\int_{T_1}^{T_M} c^S\,dT + L + \int_{T_M}^{T_2} c^L\,dT\right] \qquad (3)$$

with *m* being the plaster mass, *f* representing the mass fraction of PCMs in plaster, which was 0.5 in our case study, and T_M the melting temperature of PCMs. No variation on plaster conductivity with and without the PCM was considered in order to only tale into account the effect in terms of increased heat storage.

Finally, the effect of embodied PCM on thermal comfort was investigated by assuming the presence of at least one occupant starting from 3 PM to 8 AM, and calculating occupants' comfort conditions according to Fanger's model. In the specific "People" Energyplus object both "work efficiency" and "air velocity" were assumed to be always zero, while clothing insulation was assumed to be 1 clo during the heating season and in the two weeks before and after, 0.5 clo during the cooling season and in the two weeks before and after, and 0.75 in the remaining periods. Results were finally analysed in terms of hours in which the percentage of dissatisfied according to Fanger's model exceeded 15%.

2.3 Toxicological assays

Human alveolar basal epithelial cells (A549, ATCC® CCL-185™) were maintained in Dulbecco's Modified Eagle Medium supplemented with 10% FBS, 50 µM glutamine, supplemented 100 U/mL penicillin and 100 mg/mL streptomycin. Cells were incubated in a humidified controlled atmosphere with a 95 % to 5 % ratio of air/CO_2, at 37 °C. For viability assay, A549 cells were seeded in 96 well microplates (Constar) at concentration of $5{\cdot}10^3$ cells/well after 24 h of stabilization. The SiO_2@PEG600 NPs were added in order to obtain a final concentration of 10 µg/mL and 40 µg/mL. The exposure was conducted for 24 h, 48 h, 72 h 96 h and the viability of cells expressed as percentage of living cells respect to control was performed using the WST-8 assay (Sigma-Aldrich) following the procedure described previously [38]. For confocal acquisitions, A549 cells were incubated with NPs at different time points following the procedure described in Ref. [39]. All confocal images were acquired using LSM700 (Zeiss, Germany) confocal microscope mounted on an Axio Observer Z1 (Zeiss, Germany) inverted microscope, by using the Alpha Plan-Apochromat (Zeiss) 100 x oil-immersion with 1.46 NA.

3. Results and Discussion

3.1 PCM properties

SiO_2@PEG600 nano-particles were firstly characterized in water by TEM in order to analyze their morphology, showing that NPs were spherical and monodispersed with a size of (300 ± 15) nm (Figure 3a). DLS measurements confirmed the size of NPs (Figure 3b) showing a uniform size distribution. SEM-EDS analysis confirmed the morphology and smooth surface of NPs and further corroborated the presence of confined PCM (PEG600) in the SiO_2 NPs core. Indeed, the silicon, oxygen and carbon element peaks appeared in the graph (silicon and oxygen for silica and carbon and oxygen for PEG600) (Figure 3c,d). FT-IR analysis was conducted on the NPs samples in order to verify the presence of bonds corresponding to PEG600 and SiO_2.

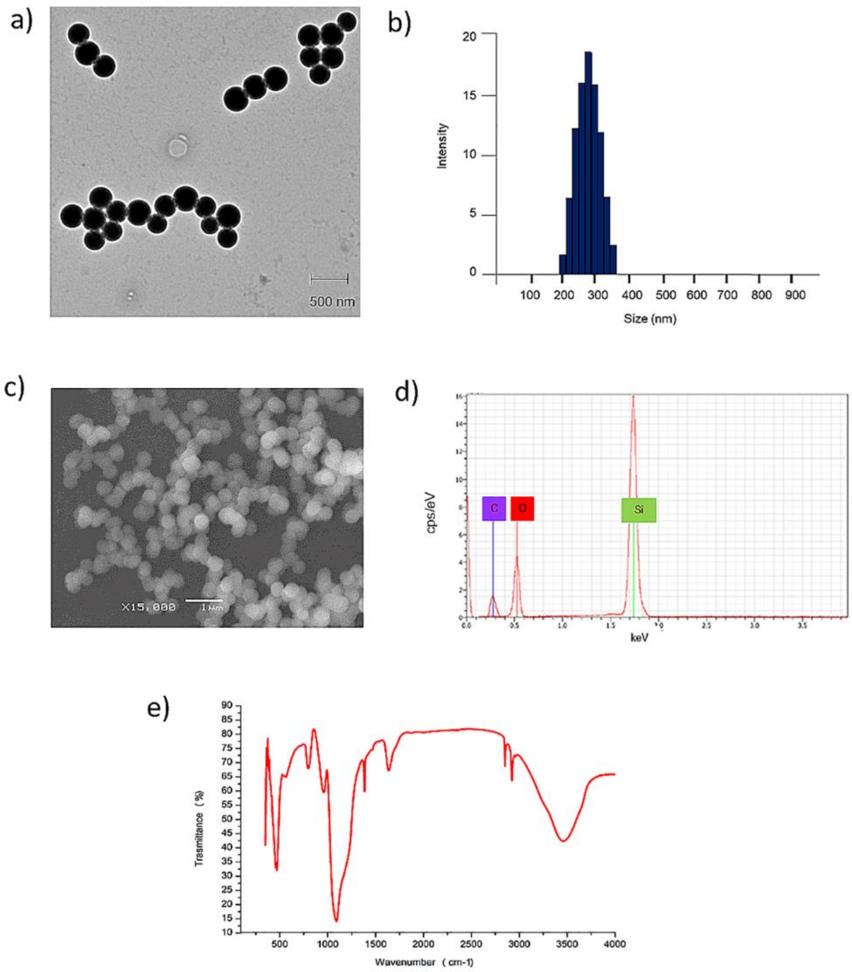

Figure 3. Characterization of SiO_2@PEG600 core/shell NPs. a. Representative image of NPs acquired by Transmission Electron Microscopy (TEM) b. Dynamic Light Scattering (DLS) measurement c. Representative image of NPs acquired by Scanning Electron Microscopy (SEM) d. Energy Dispersive X-ray Spectrometry (EDS) curve e. Fourier Transform Infrared Spectroscopy (FITR) analysis.

Figure 3e showed a broad band in the region of ~3375 cm^{-1} that corresponds to -OH stretching vibration. The vibrational bands observed at ~2917 cm^{-1} and ~2849 cm^{-1}, related to the stretching of –CH. The peak obtained at ~1633 cm^{-1} was assigned to the stretching of -OH band while the peak at ~1403 cm^{-1} was attributed to the vibration of -CH. The very strong and broad IR band at ~1111 cm^{-1}, with a shoulder at ~1188 cm^{-1} represented the Si-O-Si asymmetric stretching vibrations. The IR band at ~800 cm^{-1} and 956 cm^{-1} can be assigned to symmetric stretching vibrations of Si-O-Si and silanol groups respectively. The peak at ~474 cm^{-1} was due to O-Si-O bending vibrations.

Thermal performance of novel SiO_2@PEG600 was studied using a Differential Scanning Calorimetry (DSC) testing, providing the thermogram showed in Figure 4. The melting temperature (Tm) of the SiO_2@PEG600 NPs was found to be 21˚C, with a smooth transition starting from about 10 °C, which was similar to that of the pure PEG600 as described in a previous work [40]. Moreover, the encapsulation efficiency (*R*) is an important index, which was defined as follows [41,42]:

$$R = \frac{\Delta h_m}{\Delta h_{mPCM}} * 100\ [\%] \qquad (4)$$

where Δh_m is the specific melting enthalpy of NPs and Δh_{mPCM} is the specific melting enthalpy of the PCM in pure state. As the latter is 108.4 kJ/kg for PEG600 as measured by DSC [43] and the melting enthalpy of core shell PCMs reaches a maximum of 66.24 kJ/kg (using a concentration of 1M of PEG600) in the melting process, the resulting encapsulation efficiency was 61%. Such result was in agreement with other works [44]. The resulting enthalpy referred to core/shell NPs was used in the all the simulations that were carried out subsequently.

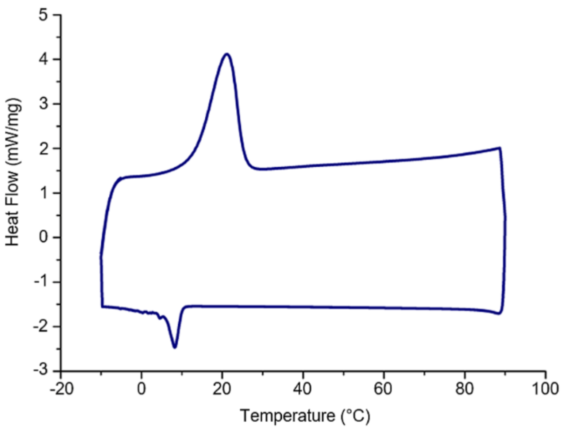

Figure 4. Differential scanning calorimetry (DSC) curve.

3.2 Energy saving potentials

The heating energy consumption per unit area was calculated, on an annual basis, using the results of the simulation process. This activity was carried out with reference to three different climatic contexts, as mentioned previously (Brindisi, Rome, Milan). The outcome of performance comparisons among the plaster containing PCMs and the standard reference plaster demonstrated that energy savings for heating could be attained in all the cases although a strong dependence on climatic conditions appeared. In fact, in Brindisi savings were 4.3%, in Rome they reduced to 2.3%, and in Milan they dropped to 1.6%. Such climatic dependence is strongly related to the different profile of outdoor temperatures and radiation patterns which finally influence the rate interior surfaces get colder. A comparison of the absolute values of yearly energy demand per unit area, as shown in Table 1, showed that that in absolute terms the largest decrease was found in Milan (0.44 kWh/m^2yr), while Rome (0.26 kWh/m^2yr) and Brindisi (0.29 kWh/ m^2yr) showed more similar results. This was due to the higher annual heating consumption in Milan and Rome as the first two cities belong to climate zones with a longer heating period, more heating hours, and lower outdoor temperatures.

Table 1. Specific energy use for heating on a yearly basis

	Brindisi		**Rome**		**Milan**	
	Ref.	PCM	Ref.	PCM	Ref.	PCM
Specific heating energy [kWh/m^2.yr]	6.92	6.63	11.64	11.38	26.80	26.36
Percent Variation [%]		-4.3%		-2.3%		-1.6%
Specific cooling energy [kWh/m^2.yr]	4.86	4.85	3.69	3.68	2.68	2.65
Percent variation [%]		-0.2%		-0.3%		-1.1%

The energy consumption for summer air-conditioning was barely affected by PCMs embodied in plaster, as shown by cooling energy comparisons (**Table 1**). In fact, results showed negligible effects due to PCMs because set-point temperatures of the cooling system was 26°C, well above the melting temperature of SiO_2@PEG600, taking place around 21 °C. Quite predictably, the same behavior was found in all the locations under investigation in this study. Figure 5 clearly shows this effect, by plotting a scatterplot of the surface temperatures (on the Southern wall, in Brindisi), of the wall with the reference treatment and the wall with PCM. Clearly, above 24 °C the temperatures converge, while they show significant variations (within a ±1°C range) between 18 and 23 °C.

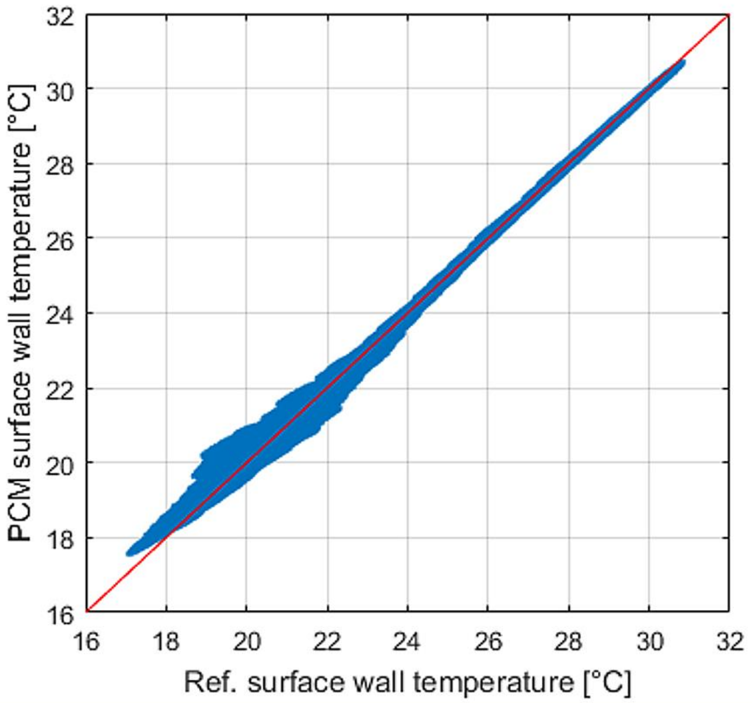

Figure 5 Scatterplot of the interior surface temperature of the Southern wall of the reference conditions vs. the same parameter on the wall treated with PCM.

In order to better understand how the surface temperature changes, depending on the season, Figure 6 shows the variation of the internal surface temperature reported on the South wall on a yearly basis for all three locations comparing the wall finished with plaster embodying PCM with the reference one. The material is completely melted in the summer season, while the difference in temperature shows a positive value in winter and autumn, in all three locations. Average difference in temperature undergoes a change of sign in spring (with a slight shift depending on the location) because the presence of the PCM delays the heating of the interior surfaces, achieving a reduction of temperatures on the wall surface, ranging around 0.5 °C in all the locations.

It can be observed that, in all cases, the main effect of the embodied PCMs consisted in a positive variation of surface temperature, particularly evident in the Autumnal period, meaning that the wall with PCM showed a higher temperature compared to the reference wall, in concurrence with the heating system activation periods. Moreover, the higher temperature of the surface of the plaster containing the PCM translated into a benefit in terms of energy saving, as found in the analysis of the heating system consumption, as well as in terms of indoor environment quality, as the mean radiant temperature gets higher and more similar to air temperature.

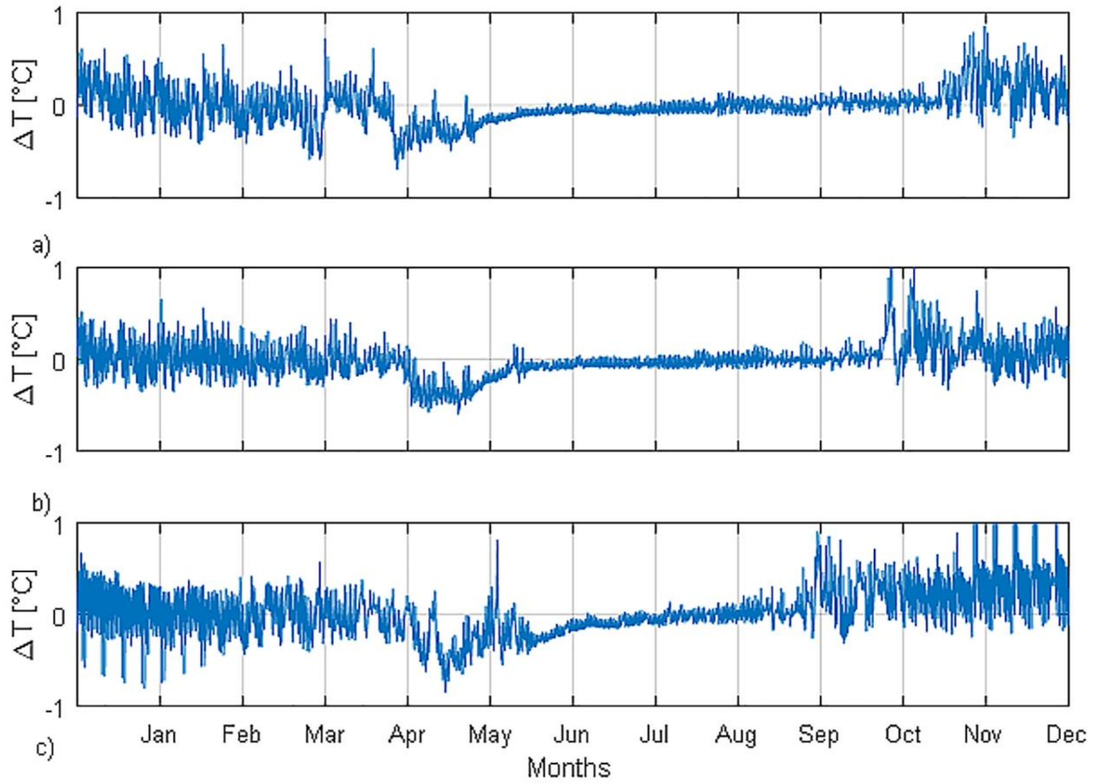

Figure 6 Variation of internal surface temperature on the South wall calculated with and without PCM in the plaster. a) Brindisi; b) Rome; c) Milan

In order to better investigate this aspect, Figure 7 shows the trends of the internal surface temperature, with and without the PCMs, along one week for each location. The week showing the highest differences between the two configurations (the reference case and the one considering plasters embodying PCMs) was selected for each location. In this way, the week with the largest temperature deviation in Brindisi was found to be from November 26th to December 2nd, with maximum differences of about 0.5°C (Figure 7a,b). Similar trends were observed for both exposed and unexposed walls, with the first having lower temperatures and being clearly affected by radiation effects. In all the cases, the PCM made the variations in temperature smoother when compared to the reference plaster. Similar conditions were observed in Rome, in the week from November 4th to November 11th (Figure 7c,d). On the other hand, in Milan, the week reporting higher surface temperature deviations was the one from October 3rd to October 10th, with temperature differences in the same range observed in the other locations (Figure 7e,f). In all cases, it was observed that the period of maximum effectiveness of the proposed phase change materials is the Autumn, with shifts depending on the climatic conditions. This fact indeed confirmed

Post-print version of the paper published in Energy and Buildings, Volumes 188–189, 1 April 2019, Pages 1-11, doi: https://doi.org/10.1016/j.enbuild.2019.02.004

that the PCM performed best at lower latitudes and milder climates, where such increased temperatures, combined with positive effects due to radiation, may lead to a shift in the time at which the heating system becomes effective.

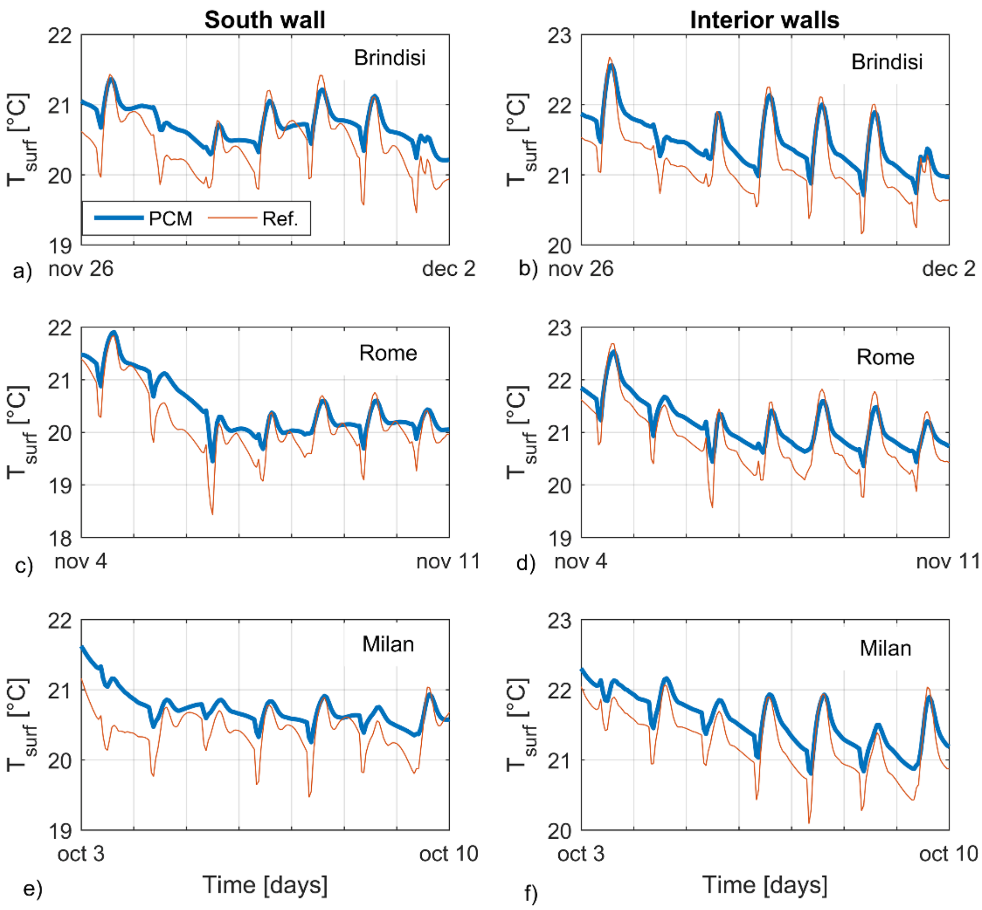

Figure 7. Graphs showing the difference in internal surface temperature of the plasters in the reference case and the one containing the new SiO_2@PEG600 material. Southern wall exposed to Sun radiation (a,c,e) and interior wall (b,d,f) were considered for the different locations: Brindisi (a,b), Rome (c,d), and Milan (e,f). For each location the week showing the greatest deviations in surface temperature was considered.

However, even in presence of the heating system, the addition of PCM to the interior walls proved to induce positive effects, particularly at the beginning and at the end of the heating season (when walls get warmer). As shown in Figure 8 in presence of a duty-cycle of the heating system, the presence of the PCM may conveniently affect the time period of the cycle, leading to a quantifiable reduction of the number of times the system is turned on. In particular, at the beginning (and at the end) of the season the period is longer and the contribution from the PCM is clearer. In February, in presence of more extreme climate conditions, the difference between the case with reference wall and that treated with PCM becomes much smaller.

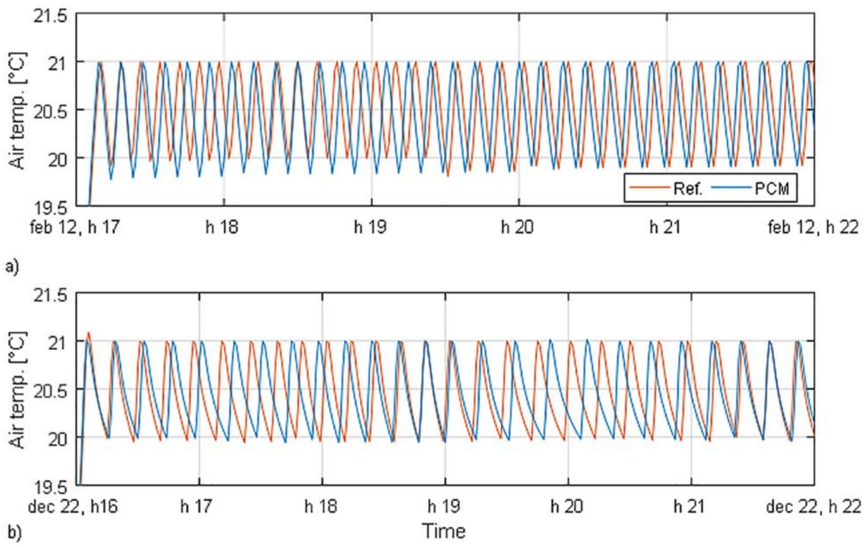

Figure 8. Plot of the indoor air temperature in Brindisi at two different times of the year: a) February 12th, b) December 22nd

Finally, the analysis of thermal comfort conditions showed (Table 2) that the addition of PCM resulted in a generalized reduction of the number of hours in which discomfort conditions are found. As expected, in Winter and Autumn a reduction of discomfort hours is observed, and it is particularly evident in Rome and Milan. During the Spring the inclusion of PCM determines a slight increase in the number of discomfort hours, as an obvious consequence of the slower increase of the interior wall temperature compared to the reference case. However, this increase is comparatively smaller than the benefits obtained during Autumn. Finally, in Summer the smallest variations appeared, quite predictably considering that the range of temperatures in which the PCM is effective is normally below room temperatures in that season. Such results confirm the usefulness of the treatment with PCM, as even in cities where their effect on energy saving is lower (like Milan), they nonetheless contribute to improve indoor comfort conditions.

Table 2. Summary of the analysis of thermal comfort conditions expressed in terms of hour in which Fanger's predicted percentage of dissatisfied (PPD) exceeds 15% as a function of season, for each of the locations under analysis.

	BR_ref	BR_PCM	Var.	RM_ref	RM_PCM	Var.	MI_ref	MI_PCM	Var.
Overall	1389	1373	–14	781	745	–36	1529	1440	–89
Winter	12	3	–9	34	10	–24	466	441	–25
Spring	84	86	2	18	21	3	174	192	18
Summer	985	978	–7	567	563	–4	185	176	–9
Autumn	308	306	–2	162	151	–11	704	631	–73

This first round of simulations focused on the concise identification of the potential benefits obtainable through the integration of the newly formulated PCM nanomaterial in building plasters. Further activities will be aimed at demonstrating other possible uses of the innovative material produced in this experimental activity; on the other hand, they will aim at improving the efficiency of encapsulation and thermal performance. Moreover, it will be possible to identify further PCMs suitable for uses related to constructions.

3.3. Toxicological analysis

In order to verify if the new synthetized nanomaterial were toxic, we exposed human alveolar basal epithelial cells (A549) to NPs since they effectively mimic the inhalation exposure. Cell viability was evaluated by means of the WST-8 assay. The treatment with SiO_2@PEG600 did not induce a dose-dependent reduction of cells viability after the treatment with 10 µg/mL and 40 µg/mL of SiO_2@PEG600, for 24h, 48h, 72h, 96h. (Figure 9a). In addition, the confocal analysis on A549 cells performed after incubation of cells with 40 µg/mL of SiO_2@PEG600 for 72h, clearly showed that there were no toxic effects on cell morphology (Figure 9b). The toxicological profile is a critical point to the use of these new nanomaterials in buildings. In this way, our new synthetized nanomaterials have not only a great thermal performance, but they are safe and can be exposed to living organisms.

Post-print version of the paper published in Energy and Buildings, Volumes 188–189, 1 April 2019, Pages 1-11, doi: https://doi.org/10.1016/j.enbuild.2019.02.004

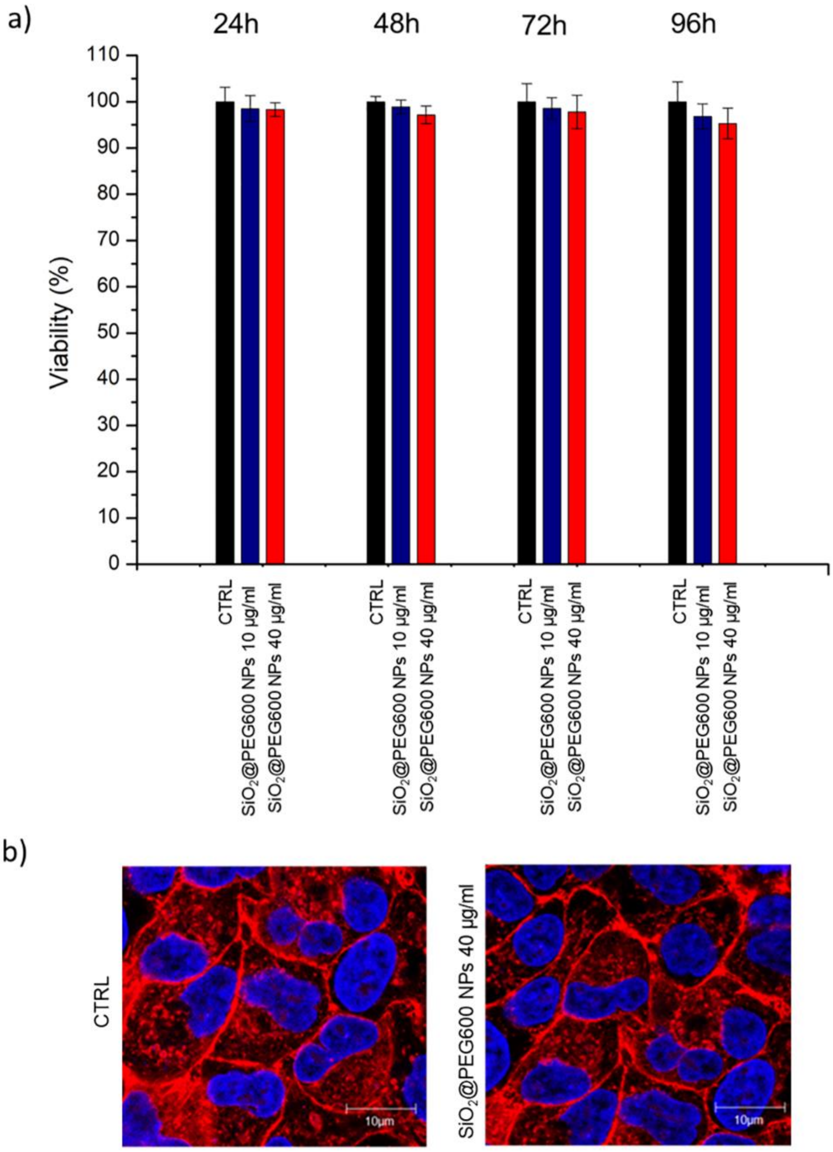

Figure 9. Toxicity assessment of SiO_2@PEG600 core/shell NPs on A549 cells. Figure 9a. Viability assay (WST-8) of A549 cells after 24 h, 48 h, 72 h and 96 h exposure to two doses (10 µg/mL and 40 µg/mL) SiO_2@PEG600 core/shell NPs. Viability of NPs-treated cells was normalized to non-treated control cells. As positive control (P), cells were incubated with 5% DMSO (data not shown). Data reported as mean ± SD from three independent experiments are considered statistically significant compared with control (n= 8) for p value < 0.05 (<0.05 *, <0.01 ** and <0.005 ***). Figure 9b. A549 were treated with 10 µg/mL and 40 µg/mL of NPs for 72 h, fixed and then stained with Phalloidin–ATTO 488 and DAPI. The 2D images of cortical actin were acquired by a Zeiss LSM700 (Zeiss) confocal microscope equipped with an Axio Observer Z1 (Zeiss) inverted microscope using a ×100, 1.46 numerical aperture oil immersion lens. All data were processed by ZEN software (Zeiss).

4. Conclusions

The nano-encapsulation of a PCM for potential use in the construction sector was investigated in this paper. In particular, in order to enhance the potential of the PCM to contribute to energy saving and thermo-regulation of the indoor temperature in buildings PEG600 was chosen because its melting temperature is close to 20°C. In addition, in order to embody this material in plasters and other building mixtures, the PCM was nano-encapsulated in a silica shell which may also contribute to enhance mechanical properties. The resulting product was analyzed under different points of view.

Better results were obtained compared to commercial microencapsulated PCMs due to the increased specific surface of silica nanoparticles, resulting in an increase of heat transfer and due to the reduced thickness of silica shells, hosting higher amounts of PCM active material in the nanoparticles core. Low-cost mass manufacturing techniques could take advantage of the proposed low-cost, low temperature solgel approach, with further chances to modify and improve nanoPCM performance, materials and morphology.

Further studies are under way in order to better understand the potential advantages resulting from the use of this material, also including its influence on mechanical properties of plasters.

Acknowledgements

A.C. kindly acknowledges the Action co-founded by Cohesion and Development Fund 2007–2013 – APQ Research Puglia Region ‘‘*Regional programme supporting smart specialisation and social and environmental sustainability – FutureInResearch*”.

Author information

Corresponding Author

*E-mail: francesco.fiorito@poliba.it

Conflict of interest

The authors declare that they have no conflict of interest.

References

[1] J. Kośny, PCM-Enhanced Building Components, 2015. doi:10.1007/978-3-319-14286-9.

[2] Z. Ma, W. Lin, M.I. Sohel, Nano-enhanced phase change materials for improved building performance, Renew. Sustain. Energy Rev. 58 (2016) 1256–1268.

doi:10.1016/j.rser.2015.12.234.

[3] A. Sharma, V. V. Tyagi, C.R. Chen, D. Buddhi, Review on thermal energy storage with phase change materials and applications, Renew. Sustain. Energy Rev. 13 (2009) 318–345. doi:10.1016/j.rser.2007.10.005.

[4] R. Baetens, B. Petter, A. Gustavsen, Phase change materials for building applications : A state-of-the-art review, 42 (2012) 1361–1368. doi:10.1016/j.enbuild.2010.03.026.

[5] W. Su, J. Darkwa, G. Kokogiannakis, Review of solid-liquid phase change materials and their encapsulation technologies, Renew. Sustain. Energy Rev. 48 (2015) 373–391. doi:10.1016/j.rser.2015.04.044.

[6] X. Min, M. Fang, Z. Huang, Y. Liu, Y. Huang, R. Wen, et al., Enhanced thermal properties of novel shape-stabilized PEG composite phase change materials with radial mesoporous silica sphere for thermal energy storage, Sci. Rep. 5 (2015) 12964. doi:10.1038/srep12964.

[7] T. Khadiran, M.Z. Hussein, Z. Zainal, R. Rusli, Advanced energy storage materials for building applications and their thermal performance characterization: A review, Renew. Sustain. Energy Rev. 57 (2016) 916–928. doi:10.1016/j.rser.2015.12.081.

[8] A. Mavrigiannaki, E. Ampatzi, Latent heat storage in building elements : A systematic review on properties and contextual performance factors, Renew. Sustain. Energy Rev. 60 (2016) 852–866. doi:10.1016/j.rser.2016.01.115.

[9] Z. Pavlík, A. Trník, J. Ondruška, M. Keppert, M. Pavlíková, P. Volfová, et al., Apparent Thermal Properties of Phase-Change Materials: An Analysis Using Differential Scanning Calorimetry and Impulse Method, Int. J. Thermophys. (2012) 851–864. doi:10.1007/s10765-012-1169-1.

[10] F. Ascione, N. Bianco, R.F. De Masi, F. de' Rossi, G.P. Vanoli, Energy refurbishment of existing buildings through the use of phase change materials: Energy savings and indoor comfort in the cooling season, Appl. Energy. 113 (2014) 990–1007. doi:10.1016/j.apenergy.2013.08.045.

[11] J. Fořt, A. Trník, Z. Pavlík, Influence of PCM Admixture on Thermal Behavior of Composite Plaster, Adv. Mater. Res. 1054 (2014) 209–214. doi:10.4028/www.scientific.net/AMR.1054.209.

[12] Z. Pavlík, A. Trník, M. Keppert, M. Pavlíková, J. Žumár, R. Černý, Experimental investigation of the properties of lime-based plaster-containing PCM for enhancing the heat-storage capacity of building envelopes, Int. J. Thermophys. 35 (2014) 767–782. doi:10.1007/s10765-013-1550-8.

[13] F. Fiorito, Phase-change materials for indoor comfort improvement in lightweight buildings . A parametric analysis for Australian climates, Energy Procedia. 57 (2014) 2014–2022. doi:10.1016/j.egypro.2014.10.066.

[14] K.O. Lee, M.A. Medina, Using phase change materials for residential air conditioning peak demand reduction and energy conservation in coastal and transitional climates in the State of California, Energy Build. 116 (2016) 69–77. doi:10.1016/j.enbuild.2015.12.012.

[15] L. Navarro, A. De Gracia, A. Castell, L.F. Cabeza, Experimental evaluation of a concrete core slab with phase change materials for cooling purposes, Energy Build. 116 (2016) 411–419. doi:10.1016/j.enbuild.2016.01.026.

[16] M. Kenisarin, K. Mahkamov, Passive thermal control in residential buildings using phase change materials, Renew. Sustain. Energy Rev. 55 (2016) 371–398. doi:10.1016/j.rser.2015.10.128.

[17] H.M. Belen Zalba, Jose Marın, Luisa F. Cabeza, Review on thermal energy storage with phase change : materials , heat transfer analysis and applications, 2003.

[18] R. Parameshwaran, S. Kalaiselvam, Nano and Biotech Based Materials for Energy Building Efficiency, in: F. Pacheco Torgal, C. Buratti, S. Kalaiselvam, C.-G. Granqvist, V. Ivanov (Eds.), Springer International Publishing, Cham, 2016: pp. 215–243. doi:10.1007/978-3-319-27505-5_8.

[19] Z. Ma, W. Lin, M.I. Sohel, Nano-enhanced phase change materials for improved building performance, Renew. Sustain. Energy Rev. 58 (2016) 1256–1268. doi:10.1016/j.rser.2015.12.234.

[20] T.-P. Teng, C.-C. Yu, Characteristics of phase-change materials containing oxide nano-additives for thermal storage., Nanoscale Res. Lett. 7 (2012) 611. doi:10.1186/1556-276X-7-611.

[21] A. Sari, C. Alkan, C. Bilgin, Micro/nano encapsulation of some paraffin eutectic mixtures with poly(methyl methacrylate) shell: Preparation, characterization and latent heat thermal energy storage properties, Appl. Energy. 136 (2014) 217–227. doi:10.1016/j.apenergy.2014.09.047.

[22] M.K. Moghaddam, S.M. Mortazavi, T. Khaymian, Micro/nano-encapsulation of a phase change material by coaxial electrospray method, Iran. Polym. J. 24 (2015) 759–774. doi:10.1007/s13726-015-0364-x.

[23] C. Liu, Z. Rao, J. Zhao, Y. Huo, Y. Li, Review on nanoencapsulated phase change materials: Preparation, characterization and heat transfer enhancement, Nano Energy. 13 (2015) 814–826. doi:10.1016/j.nanoen.2015.02.016.

[24] A. Sari, C. Alkan, D. Kahraman Döğüşcü, A. Biçer, Micro/nano-encapsulated n-heptadecane with polystyrene shell for latent heat thermal energy storage, Sol.

Energy Mater. Sol. Cells. 126 (2014) 42–50. doi:10.1016/j.solmat.2014.03.023.

[25] G. Fang, Z. Chen, H. Li, Synthesis and properties of microencapsulated paraffin composites with SiO2shell as thermal energy storage materials, Chem. Eng. J. 163 (2010) 154–159. doi:10.1016/j.cej.2010.07.054.

[26] V. De Matteis, A. Cannavale, A. Coppola, F. Fiorito, Nanomaterials and Smart Nanodevices for Modular Dry Constructions: The Project “easy House,” in: Procedia Eng., 2017. doi:10.1016/j.proeng.2017.04.230.

[27] W.T. Chan, C.C. Liu, J.S.C. Chiau, S.T. Tsai, C.K. Liang, M.L. Cheng, et al., In vivo toxicologic study of larger silica nanoparticles in mice, Int. J. Nanomedicine. 12 (2017) 3421–3432. doi:10.2147/IJN.S126823.

[28] K.S. Finnie, D.A. Jacques, M.J. McGann, M.G. Blackford, C.J. Barbé, Encapsulation and controlled release of biomolecules from silica microparticles, J. Mater. Chem. 16 (2006) 4494–4498. doi:10.1039/b611840b.

[29] H. Zhang, X. Wang, D. Wu, Silica encapsulation of n-octadecane via sol-gel process: A novel microencapsulated phase-change material with enhanced thermal conductivity and performance, J. Colloid Interface Sci. 343 (2010) 246–255. doi:10.1016/j.jcis.2009.11.036.

[30] G. V. Belessiotis, K.G. Papadokostaki, E.P. Favvas, E.K. Efthimiadou, S. Karellas, Preparation and investigation of distinct and shape stable paraffin/SiO2composite PCM nanospheres, Energy Convers. Manag. 168 (2018) 382–394. doi:10.1016/j.enconman.2018.04.059.

[31] S. Tahan Latibari, M. Mehrali, M. Mehrali, T.M. Indra Mahlia, H.S. Cornelis Metselaar, Synthesis, characterization and thermal properties of nanoencapsulated phase change materials via sol-gel method, Energy. 61 (2013) 664–672.

doi:10.1016/j.energy.2013.09.012.

[32] C.B. Wu, G. Wu, X. Yang, Y.J. Liu, C.X. Gao, Q.H. Ji, et al., Preparation of Mannitol@Silica core-shell capsules via an interfacial polymerization process from water-in-oil emulsion, Colloids Surfaces A Physicochem. Eng. Asp. 457 (2014) 487–494. doi:10.1016/j.colsurfa.2014.06.018.

[33] V. Pethurajan, S. Sivan, A.J. Konatt, A.S. Reddy, Facile approach to improve solar thermal energy storage efficiency using encapsulated sugar alcohol based phase change material, Sol. Energy Mater. Sol. Cells. 185 (2018) 524–535. doi:10.1016/j.solmat.2018.06.007.

[34] S.U.S. Climates, J. Kosny, N. Shukla, A. Fallahi, Cost Analysis of Simple Phase Change Material-Enhanced Building Envelopes in, (2013). http://www.nrel.gov/docs/fy13osti/55553.pdf.

[35] P.L. Turecek, M.J. Bossard, F. Schoetens, I.A. Ivens, PEGylation of Biopharmaceuticals: A Review of Chemistry and Nonclinical Safety Information of Approved Drugs, J. Pharm. Sci. 105 (2016) 460–475. doi:10.1016/j.xphs.2015.11.015.

[36] K. Knop, R. Hoogenboom, D. Fischer, U.S. Schubert, Poly(ethylene glycol) in drug delivery: Pros and cons as well as potential alternatives, Angew. Chemie - Int. Ed. 49 (2010) 6288–6308. doi:10.1002/anie.200902672.

[37] W. Stober, A. Fink, Controlled Growth of Monodispersed Silica Spheres in the Micron Size Range, J. Colloid Interface Sci. 26 (1968) 62–69. doi:10.1016/0021-9797(68)90272-5.

[38] V. De Matteis, L. Rizzello, M.P. Di Bello, R. Rinaldi, One-step synthesis, toxicity assessment and degradation in tumoral pH environment of SiO2@Ag core/shell

nanoparticles, J. Nanoparticle Res. 19 (2017). doi:10.1007/s11051-017-3870-2.

[39] V. De Matteis, M.A. Malvindi, A. Galeone, V. Brunetti, E. De Luca, S. Kote, et al., Negligible particle-specific toxicity mechanism of silver nanoparticles: The role of Ag+ ion release in the cytosol, Nanomedicine Nanotechnology, Biol. Med. 11 (2015) 731–739. doi:10.1016/j.nano.2014.11.002.

[40] S. Ghosh, P. Bhatkhande, Encapsulation of PCM for Thermo-Regulating Fabric Application, Int. J. Org. Chem. 2 (2012) 366–370. doi:10.4236/ijoc.2012.24050.

[41] K. Tumirah, M.Z. Hussein, Z. Zulkarnain, R. Rafeadah, Nano-encapsulated organic phase change material based on copolymer nanocomposites for thermal energy storage, Energy. 66 (2014) 881–890. doi:10.1016/j.energy.2014.01.033.

[42] X. Niu, Q. Xu, Y. Zhang, Y. Zhang, Y. Yan, T. Liu, Fabrication and Properties of Micro-Nanoencapsulated Phase Change Materials for Internally-Cooled Liquid Desiccant Dehumidification, Nanomaterials. 7 (2017) 96. doi:10.3390/nano7050096.

[43] T. Khadiran, M. Zobir, Z. Zainal, R. Rusli, Advanced energy storage materials for building applications and their thermal performance characterization : A review, Renew. Sustain. Energy Rev. 57 (2016) 916–928. doi:10.1016/j.rser.2015.12.081.

[44] Y. Fang, X. Liu, X. Liang, H. Liu, X. Gao, Z. Zhang, Ultrasonic synthesis and characterization of polystyrene/n-dotriacontane composite nanoencapsulated phase change material for thermal energy storage, Appl. Energy. 132 (2014) 551–556. doi:10.1016/j.apenergy.2014.06.056.